Journal of Catalysis 279 (2011) 220–228

Contents lists available at ScienceDirect

Journal of Catalysis

journal homepage: www.elsevier.com/locate/jcat

Monomolecular cracking of propane over acidic chabazite: An ab initio molecular dynamics and transition path sampling study

Tomáš Bučko [a,b,c,*], Lubomir Benco [b,c], Jürgen Hafner [c], János G. Ángyán [d]

[a] Department of Physical and Theoretical Chemistry, Faculty of Natural Sciences, Comenius University, Mlynská Dolina, SK-84215 Bratislava, Slovakia
[b] Institute of Inorganic Chemistry, Slovak Academy of Sciences, Dubravska Cesta 9, SK-84236 Bratislava, Slovakia
[c] Fakultät für Physik and Center for Computational Materials Science, Universität Wien, Sensengasse 8/12, A-1090 Wien, Austria
[d] Équipe de Modélisation Quantique et Cristallographique, CRM2, Institut Jean Barriol, UMR 7036, CNRS – Nancy-Université, B.P. 239, F-54506 Vandœuvre-lès-Nancy, France

ARTICLE INFO

Article history:
Received 9 December 2010
Revised 20 January 2011
Accepted 22 January 2011
Available online 24 February 2011

Keywords:
Acidic zeolites
Alkane cracking
Ab initio
Molecular dynamics
Transition path sampling
Entropy effect

ABSTRACT

The monomolecular Haag–Dessau mechanism for propane cracking over acidic chabazite has been studied using dispersion-corrected periodic DFT calculations in combination with ab initio molecular dynamics (AIMD) simulations, transition path sampling (TPS), and free-energy integrations. The AIMD simulations show that due to the weak specific interaction of the saturated molecule with Brønsted acid sites, the adsorption energy is considerably reduced at elevated temperature and that only a fraction of the molecules adsorbed within the zeolite is sufficiently close to the acid site to form a reactant complex for protonation. TPS shows that the preferred reaction mechanism is the protonation of a terminal methyl group. The direct proton attack on the C–C bond between the methyl and methylene groups is not excluded but occurs with lower probability. The intrinsic reaction parameters such as free energy and entropy of activation are determined using thermodynamic integration based on constrained molecular dynamics simulations.

1. Introduction

Cracking is a chemical reaction in which hydrocarbons are broken into shorter fragments. An industrially important example of hydrocarbon cracking is the conversion of heavy fractions of crude oil to more valuable light fractions used, e.g., for fuel production. The reaction can be catalyzed by solid acids such as zeolites [1]. The reaction mechanism for the cracking of saturated hydrocarbons depends on the thermodynamic conditions. The classical mechanism [2,3] is a chain reaction in which carbenium ions play a central role. The bond in the β-position with respect to the positively charged trivalent carbon atom is broken, leading to the formation of shorter molecules – an alkane and a carbenium cation. The carbenium cation can abstract a hydride from another alkane, forming a new carbenium cation. Initially, carbenium ions can be created, for instance, by protonation of alkenes that may be present in the feed as impurities.

At specific conditions, such as low partial pressure of the reactant and high reaction temperature ($T > 600$ K) [4], and only at such conditions, the alternative monomolecular Haag–Dessau mechanism is favored. Monomolecular cracking of an alkane produces an alkane with a shorter C–C chain and an alkene. Alkenes are stronger proton acceptors than alkanes. When a sufficiently high concentration of alkenes is created, the classical mechanism prevails. Hence, the monomolecular mechanism can be active only at a low partial pressure of the reactant. Another factor that affects the cracking mechanism is the zeolite geometry. It is known that in zeolites with small pores, such as erionite, bimolecular cracking is hindered by sterical constraints [5].

The reaction mechanism for a monomolecular cracking has been thoroughly investigated both experimentally [5–14] and theoretically [15–25]. The reaction proceeds in two steps [15] shown in Scheme 1: (i) Protonation of the alkane at an acid site, followed by creation of a carbonium cation, and (ii) collapse of the carbonium ion leading to the formation of an alkane and an alkene. The rate-determining step is (i) with a measured (apparent) activation energy of $\Delta E^{\ddagger}_{meas}$ decreasing for short linear alkanes from 155 to 105 kJ/mol with increasing carbon number from C_3 to C_6 [7]. This means that the reactivity of linear alkanes increases significantly with increasing chain length. If one defines a quantity $\Delta E^{\ddagger}_{int} = \Delta E^{\ddagger}_{meas} - \Delta H_{ads}$ often identified with an intrinsic activation barrier in the literature [12–14], analysis of experimental data indicates that the intrinsic barrier is almost constant in a homologue series of alkanes, e.g., approximately equal to 200 kJ/mol for zeolite H-ZSM5. Similar relation has been reported for other types of zeolites [10–12,14], which suggests that the ability of a Brønsted site to transfer a proton to an alkane does not vary significantly [11].

* Corresponding author at: Department of Physical and Theoretical Chemistry, Faculty of Natural Sciences, Comenius University, Mlynská Dolina, SK-84215 Bratislava, Slovakia. Fax: +421 2 60286231.
E-mail address: tomas.bucko@univie.ac.at (T. Bučko).

0021-9517/$ - see front matter © 2011 Elsevier Inc. All rights reserved.
doi:10.1016/j.jcat.2011.01.022

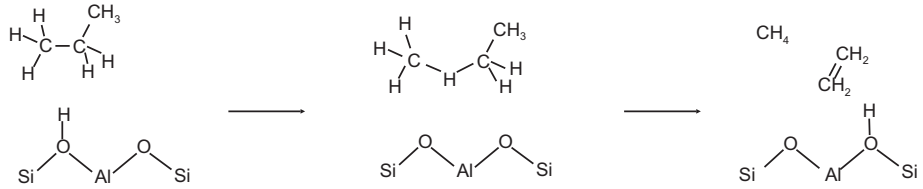

Scheme 1. Mechanism for monomolecular cracking of propane.

Hence, the reactant heat of adsorption would become the dominant factor determining the variation of cracking activity with chain length of the alkane, on the one hand, and zeolite pore shape, on the other. Recently, such an interpretation of the experimental data has been debated [13,14].

Most theoretical investigations into cracking reactions using density functional theory (DFT) presented so far concentrate on the calculation of the activation energy required for the protonation of an alkane and hence ignore the effects of the adsorption thermodynamics – essentially it is assumed that all molecules are also in a reactant state where they can be protonated. All calculations use very small clusters (with 3–5 tetrahedral sites) to represent the zeolite and either gradient-corrected [17,18] or hybrid [22–25] exchange-correlation functionals. Rigby et al. [19] performed cluster calculations at the Hartree–Fock level and attempted to account for correlation effects by performing second-order MP2 perturbation corrections at fixed geometry. The use of small clusters does not permit to account for the flexibility of the zeolitic framework, and density functional calculations do not account for dispersion forces that are known to be essential for achieving accurate adsorption energies for saturated hydrocarbons [26].

Very recently, a hybrid approach to the theoretical simulation of alkane cracking in zeolites has been presented by Swisher et al. [25]. The adsorption thermodynamics has been studied using configurational-bias Monte Carlo (CBMC) simulations and empirical force fields to describe the interaction between the alkane and the zeolite, while ab initio density functional calculations in combination with harmonic transition state theory (hTST) have been made to determine the intrinsic activation energies and rate coefficients for the cracking process. The important result of the first part of these investigations is that at the high temperatures characteristic for monomolecular cracking only a small fraction of the molecules adsorbed in the cavity of the zeolite are sufficiently close to the Brønsted site to be in a reactant state for protonation. In the ab initio calculations, the cluster approximation and the choice of the exchange-correlation functional have been critically examined. It has been found that increasing the cluster size from 5 to 23 tetrahedral sites at a given level of theory decreases the activation barrier for propane cracking by 34–70 kJ/mol. The results of periodic calculations were also reported, but as the cluster calculations used a hybrid functional whereas the periodic calculations were based on a gradient-corrected functional, it was not possible to decide whether the results with the large cluster were already converged to the periodic limit. Calculations using the small clusters show an activation energy for propane increasing with a higher level of theory (from hybrid functionals to MP2), while calculations for the large cluster suggest a much smaller influence of the theoretical approach and a decrease rather than increase in the activation energy at a higher level of theory. For all alkanes, the intrinsic activation entropies were found to be negative, with a tendency to become even more negative with increasing chain length. This is in contrast to the conclusions of Bhan et al. [13].

The main focus of the work of Swisher et al., however, was to investigate the kinetics of alkane cracking. Monte Carlo calculations of the thermodynamics were made with the intrinsic rate coefficients derived from DFT calculations on the small clusters and absolute rate theory. The qualitative trend of the dependence of the reaction rate on carbon number was reproduced, but the calculated rate coefficients were found to be a factor of 10–100 smaller than observed. The discrepancy was attributed to the use of the small T5 cluster, because limited results for the larger T23 cluster revealed a significant improvement.

In this work, we study in detail the monomolecular cracking of propane over acidic chabazite using periodic DFT calculations including dispersion corrections. We have performed ab initio molecular dynamics simulations for the characterization of the adsorption at finite temperatures, transition path sampling (TPS) for the identification of the reaction path, and free-energy gradient integrations for the determination of the free energies of activation. The use of advanced statistical-mechanical approaches in combination with dispersion-corrected ab initio calculations permits to explore the influence of the dynamical properties of reactants, products, and zeolite host on the reaction.

2. Methodology

2.1. Structural model

Our calculations were performed for acidic chabazite with one acid proton and one Al site per a simulation cell. The acid proton was located in position O4 according to the nomenclature of Jeanvoine et al. [27]. The lattice parameters have been derived from the experimental geometry determined for a highly siliceous form (SSZ-13) of chabazite [28] ($R\bar{3}$ m, $a = 9.291$ Å, $\alpha = 93.92°$). In order to avoid undesired interactions between the periodically repeated images of the reactive domain containing the acid site and the hydrocarbon molecule, a larger simulation cell has been used. The lattice vectors of the larger cell ($\mathbf{a},\mathbf{b},\mathbf{c}$) are related to those of the unit cell ($\mathbf{a}_1,\mathbf{a}_2,\mathbf{a}_3$) via $\mathbf{a} = \mathbf{a}_1 + \mathbf{a}_2$,$\mathbf{b} = \mathbf{a}_1 - \mathbf{a}_2$, and $\mathbf{c} = \mathbf{a}_3$, leading to a cell with lattice parameters $a = 12.682$ Å, $b = 13.581$ Å, $c = 9.291$ Å, $\alpha = 90.00°$, $\beta = 95.74°$, and $\gamma = 90.00°$. The shortest distance between atoms from reactive domain and their repeated images is greater than 5 Å. The periodically repeated cell contains 24 tetrahedral units: one AlO_4 and 23 SiO_4 tetrahedra.

2.2. Electronic structure calculation

Periodic DFT calculations have been made using the VASP code [29–32]. The Kohn–Sham equations have been solved variationally in a plane-wave basis set using the projector-augmented-wave (PAW) method of Blöchl [33], as adapted by Kresse and Joubert [34]. The exchange-correlation energy was described by the PBE generalized gradient approximation [35]. Brillouin-zone sampling was restricted to the Γ-point. The plane-wave cutoff was set to 300 eV. The convergence criterion for the electronic self-consistency cycle, measured by the change in the total energy between successive iterations, was set to 10^{-4} eV/cell.

2.3. Dispersion corrections – the DFT-D2 approach

Standard DFT functionals fail to describe van der Waals interactions [26]. As a significant part of the interaction energy between alkanes and a zeolite is due to van der Waals interactions [36], we adopted semi-empirical approach of Grimme [37] implemented in the VASP code [38] in which dispersion corrections to the DFT total energies and forces are approximated by semiempirical pairwise potentials of the form[1]:

$$E_{\mathrm{disp}} = -\frac{s_6}{2}\sum_{i=1}^{N_{at}}\sum_{j=1}^{N_{at}}\sum_{L}{}' \frac{C_6^{ij}}{|r^{i,0}-r^{j,L}|^6} f_{dmp}(|r^{i,0}-r^{j,L}|), \quad (1)$$

The summations in Eq. (1) are over all atoms N_{at} and all translations of the unit cell $L = (l_1, l_2, l_3)$, the prime indicates that $i \neq j$ for $L = 0$, s_6 is a global scaling factor depending on the chosen exchange-correlation functional, C_6^{ij} denotes the dispersion coefficient for the atom pair ij, $r^{j,L}$ is the position vector of atom i after performing L translations of the unit cell along lattice vectors. The damping function:

$$f_{dmp}(r_{ij}) = \frac{1}{1+e^{-d(r_{ij}/r_0^{ij}-1)}} \quad (2)$$

scales the force field such as to provide only negligible contribution to dispersion energy for distances within typical bonding situations. The combination rules for parameters C_6 and r_0 are $C_6^{ij} = \sqrt{C_6^i C_6^j}$, and $r_0^{ij} = (r_0^i + r_0^j)$, where C_6^i and r_0^i are dispersion coefficient, and effective van der Waals radius for an atom i, respectively.

Parameters optimized for the use in combination with the PBE functional have been used in this study [37]. The DFT-D2 approach was recently shown to improve predictions on structure, energetics, and elastic properties of wide range of materials where dispersion forces play an important role [38].

2.4. Geometry optimizations and static transition state searches

Transition states on the potential energy surface have been identified using the dimer method [39], as recently improved by Heyden et al. [40]. Atomic positions were considered to be relaxed if all forces acting on the atoms were smaller than 0.03 eV/Å. Transition states were proven to be first-order saddle points of the potential energy surface using vibrational analysis. The potential energy minima have been optimized using a conjugate gradient algorithm [41].

2.5. Molecular dynamics and the free energy calculations

Born–Oppenheimer molecular dynamics simulations have been performed in the NVT ensemble. The simulation temperature has been controlled using a Nosé–Hoover thermostat [42,43]. An integration step of 1 fs has been used. The atomic mass of tritium has been used for all H atoms in order to narrow the vibrational spectrum and thus to avoid the thermal separation of "hard" and "soft" vibrational modes. The free-energy reaction profiles have been calculated using the thermodynamic integration technique [44–47] as described in our earlier work on proton transfer reactions [48]. A brief description of the method can be found in Appendix A.

2.6. Transition path sampling

Transition path sampling (TPS) [49] is a computational method based on molecular dynamics designed to study rare events such as chemical reactions and phase transitions. In TPS, the space of reactive trajectories is sampled by performing trial moves such as "shooting" and "shifting". Sampling is ergodic – the relative number of reactive trajectories corresponding to different reaction mechanisms is proportional to their relative likelihood in the reactive trajectories space. The TPS technique allows to study reaction mechanisms in unbiased way; for a recent application to the dehydrogenation of alkanes catalyzed by zeolite, see Ref. [50]. Some details on TPS are presented in Appendix B; for in-depth description of the method, see Ref. [49].

3. Limitations of static transition path searches

A number of theoretical studies [15–25] have been devoted to the investigation into the monomolecular cracking reaction of short alkanes catalyzed by zeolites. To the best of our knowledge, all previous theoretical studies used a static approach based on the analysis of potential energy surfaces to determine intrinsic activation energy of reaction. In this approach, minima on the potential energy surface represent reactant, product, and intermediate states and saddle points represent transition states. The reaction barrier is computed as the energy difference between saddle point and minimum connected by a path described by an intrinsic reaction coordinate. This computationally relatively inexpensive approach can provide useful information about likely reaction paths, especially in the case of potential-energy dominated chemical reactions. Unfortunately, the application of this technique to study alkane conversion reactions in zeolites is problematic, for different reasons. In small structural models such as 3T or 5T clusters that are often used in theoretical studies to represent the zeolite [15–20,22–24], only a small number of stationary states representing possible reactant and transition states exist. With increasing complexity of the structural model, the potential energy surface becomes more and more complicated and contains many local minima and saddle points. In a realistic structural model, many different configurations for reactant and transition states exist, differing in the orientation of the alkane molecule with respect to the zeolite framework. For each such configuration, a slightly different activation energy would be computed.

We demonstrate this at the example of propane in acidic chabazite. A set of different initial configurations for a transition state search for a cracking reaction has been generated using constrained molecular dynamics. Each of these initial configurations has been optimized using the improved dimer method [40]. In such a way, eight different saddle point configurations have been identified, and three examples of transition structures are shown in Fig. 1. The reactant (R) and reaction intermediate (RI) configurations formed in the first reaction step of protolytic cracking (see Scheme 1) have been identified using a procedure in which the transition structures were distorted slightly along the direction of the eigenvector of the unstable vibrational mode (the one with an imaginary vibrational frequency) and subsequently relaxed using a conjugate gradient algorithm [41]. This procedure guarantees that minima and transition states lie on the same reaction path. The reactant and intermediate configurations linked with the transition states shown in Fig. 1 are displayed in Figs. 2 and 3, respectively. A comparison of the TS and RI configurations shows that all configurations correspond to late transition structures that are known to dominate monomolecular alkane cracking reactions [21–23,51].

We emphasize that all of these reaction paths correspond to the same reaction mechanism, and all these configurations differ only in the position and orientation of propane with respect to the zeolite framework. The total energies for the eight transitions states (TS), reactant (R), and intermediate structures (RI) are listed in Table 1. The transition state energies vary in the interval from −639.306 to −639.519 eV, i.e., the difference between the highest and lowest transition state energies is as large as 20 kJ/mol.

[1] In Ref. [38], the Eq. (1) is misprinted and a factor of 1/2 is missing

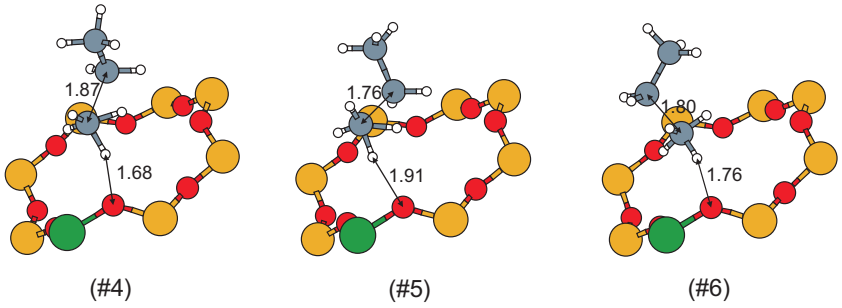

Fig. 1. Three different transition states for propane cracking. Selected interatomic distances are in Å. Corresponding potential energies are listed in Table 1.

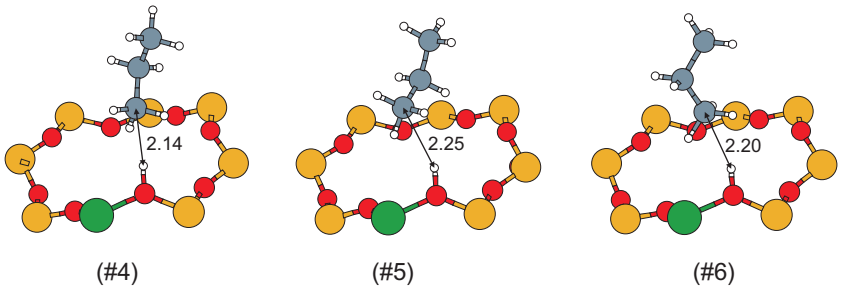

Fig. 2. Three different reactant configurations – adsorption complexes of propane at Brønsted acid site. Selected interatomic distances are in Å. Corresponding potential energies are listed in Table 1.

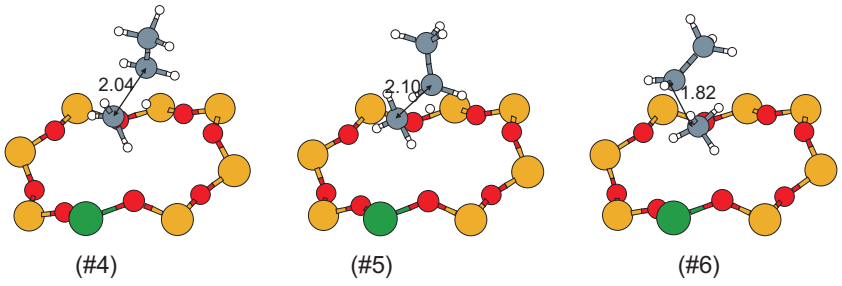

Fig. 3. Three different reaction intermediates for propane cracking over Brønsted acid site. Selected interatomic distances are in Å. Corresponding potential energies are listed in Table 1.

Table 1
Potential energies for eight different reactant (R) states, corresponding transition structures (TS), and reaction intermediates (RI) identified for protolytic propane cracking. Adsorption energies ΔE_{ads} are calculated relative to the gas-phase molecule and the unloaded zeolite. For reader's convenience, the intrinsic activation energies for forward ($\Delta E^{\ddagger}_{\rightarrow}$) and reverse ($\Delta E^{\ddagger}_{\leftarrow}$) reaction modes are listed.

Configuration	E(R) eV	ΔE_{ads} kJ/mol	E(TS) eV	$\Delta E^{\ddagger}_{\rightarrow}$ (kJ/mol)	E(RI) eV	$\Delta E^{\ddagger}_{\leftarrow}$ (kJ/mol)
1	−641.521	−65	−639.373	207	−639.389	2
2	−641.540	−67	−639.357	211	−639.422	6
3	−641.472	−60	−639.519	188	−639.623	10
4	−641.510	−64	−639.369	207	−639.410	4
5	−641.448	−58	−639.306	206	−639.413	10
6	−641.483	−61	−639.477	194	−639.497	2
7	−641.538	−67	−639.415	205	−639.475	6
8	−641.575	−70	−639.437	206	−639.485	5

Energies of reactants and intermediates are distributed over slightly narrower intervals, see Table 1. As a consequence, the intrinsic activation energies $\Delta E^{\ddagger}$ vary between 188 and 211 kJ/mol. These results can be compared with the recent calculations of Swisher et al. [25] who determined $\Delta E^{\ddagger}$ at different levels of theory and using different structural models. Using MP2 method, activation energies of 264 kJ/mol and 192 kJ/mol were calculated for a small 5T and a large 23T cluster representing H-ZSM-5, respectively. Using a hybrid functional (B3LYP), the corresponding values are 235 kJ/mol and 202 kJ/mol, while using a conventional semi-local functional (PBE) a lower value of 173 kJ/mol was calculated for a periodic zeolite structure (H-ZSM-5).

Note that all these theoretical values are significantly higher than the experimental activation energy of 155 kJ/mol reported by Narbeshuber et al. [7]. The computed adsorption energy of propane in acidic chabazite ranges from −58 to −70 kJ/mol, and the experimental heat of adsorption for propane measured at room temperature is −27 to −49 kJ/mol depending on the geometry of the internal surfaces of the acidic zeolite [36,52,53]. The reason for the disagreement between theory and experiment is that at finite temperature many different adsorption configurations occur with finite probability. As we shall demonstrate in the next section, agreement between theoretical and experimental adsorption energies improves significantly when thermal effects are taken into account. As the number of soft degrees of freedom such as a skeletal C–C–C–C torsions increases with the chain length of the alkane, it is to be expected that the uncertainty in the computed adsorption

and activation energies increases with the number of C atoms in a linear hydrocarbon. All these results indicate that neither the reactant nor the transition state can be represented with sufficient accuracy by a single configuration determined by a static relaxation. Instead, any state on the reaction path must be represented by an ensemble average representative for the reaction conditions.

4. Ab initio molecular dynamics simulation of adsorption complexes

To initiate a cracking reaction, the acidic proton must be transferred from the Brønsted site to the hydrocarbon molecule. Such a transfer is possible only if at least one of the carbon atoms of the molecule approaches the acid site to a sufficiently close distance. The probability to form an adsorption complex depends on the interplay of two opposite factors: the specific interaction between the zeolite OH group and the hydrocarbon molecule tends to stabilize structures with short C···HO distances <3.0 Å and thermal disorder tends to drive the molecule away from the acid site. It is well known from experiment [36] that the interaction of a saturated hydrocarbon with the acid site is weak, the specific interaction energy being only ∼10 kJ/mol (note that this value is well reproduced by DFT calculations [26]). The largest part of the adsorption energy arises from the interaction between the molecule and the zeolite wall mediated by dispersion forces (added here as corrections to the Hellmann–Feynman forces calculated within DFT) which do not confine the molecule to remain close to the Brønsted site. Entropy, on the other hand, increases with increasing amplitude of the translational and rotational motions of the alkane in the cavity. To investigate the impact of thermal effects on the formation of adsorption complexes, we have performed ab initio molecular dynamics simulations at three different temperatures: 100, 300, and 800 K. The total simulation time for each MD run was 100 ps. The formation of an adsorption complex has been identified by measuring the distance between the acid proton and the nearest carbon atom of propane ($r_{C\cdots H'}$). In Fig. 4, the probability distribution $P(r_{C\cdots H'})$ is shown at the three different simulation temperatures. At the lowest temperature T = 100 K, the specific C···HO interaction is the dominant factor. Propane forms a stable adsorption complex with the Brønsted acid site, and the shortest C···H′ distance was less than 3 Å for 99% of the simulation time. The distribution function $P(r_{C\cdots H'})$ shows a rather narrow peak centered at ∼2.2 Å. The internal energy of adsorption has been computed using:

$$\Delta U_{ads}(T) = \langle E_{zeo+prop}\rangle_T - \left(\langle E_{prop}\rangle_T + \langle E_{zeo}\rangle_T\right) \quad (3)$$

where $\langle E_{zeo+prop}\rangle_T$,$\langle E_{prop}\rangle_T$, and $\langle E_{zeo}\rangle_T$ are the average total (potential and kinetic) energies at the simulation temperature computed for propane adsorbed in zeolite, propane in vacuum, and the clean acidic zeolite, respectively, computed in three separate MD simulations for each temperature. As expected, the internal energy of adsorption computed for T = 100 K is similar to the interaction energies obtained by atomic relaxations (see Table 1), ΔU_{ads}= − 59 kJ/mol. At T = 300 K, thermal disorder plays already a significant role and the probability to find a carbon atom at distance shorter than 3 Å from proton decreases to 68%. Consequently, the internal energy of adsorption decreases to −44 kJ/mol. This value compares reasonably well with the experimental heat of adsorption of −47 kJ/mol measured for propane adsorbed at T = 348 K at a zeolite with a framework density similar to chabazite (H-KFI) [52]. Finally, at a temperature of 800 K, at which cracking reaction actually occurs, propane spends only ∼18% of time in a state with the shortest $C\cdots H'$ distance ⩽3 Å and the internal energy of adsorption decreases to −38 kJ/mol. At all simulation temperatures, propane tends to form adsorption complexes via one of the terminal methyl groups, while

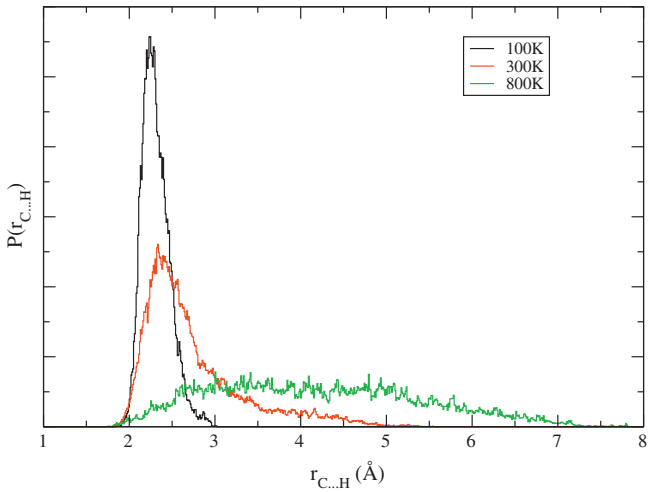

Fig. 4. Distribution function for the distance between proton and the nearest carbon atom of propane ($P(r_{C\cdots H})$) computed for three different temperatures.

the probability that the central methylene group comes sufficiently close to the proton is very low. Our conclusion that the probability to find a molecule adsorbed within the zeolite in a reactant state is rather low at reaction conditions agrees with the configurational-bias Monte Carlo simulations of Swisher et al. [25], who also found very similar values for the adsorption energy. This result also shows that the adsorption process is temperature sensitive: propane is bound to the BA site in a typical adsorption state at low temperature, while at high temperature, the adsorption complex is less stable and the motion of propane in the cavity is much less restricted. This example shows that the adsorption process is qualitatively different at low and high temperature. Hence, in contrast to usual assumptions [13,14], the entropy of adsorption cannot be considered to be temperature independent.

5. High-temperature reaction mechanism

For the monomolecular cracking of propane, two different realizations of the first reaction step can be considered [17]. In the mechanism shown in Scheme 2a, the proton (H′) attacks directly the C–C bond to be broken and all other C–H bonds remain unchanged. This mechanism has been reported, for instance, in Refs. [15,16,22–24]. In the alternative mechanism (Scheme 2b), H′ is attached to a terminal methyl group. A different hydrogen atom is shifted from the terminal carbon atom toward a carbon in the CH_2 group to form a C–H bond, and at the same time, the bond between the methyl and methylene groups is broken. Using DFT cluster calculations, Blaszkowski et al. [17] found that for ethane cracking the potential energy barriers along the two reaction paths are the same. The rate constants computed using harmonic transition state theory (hTST) indicate, however, that the mechanism (a) is slightly more advantageous. Similar reaction mechanism has been identified for the *n*-butane cracking in theoretical work of Boronat et al. [20]. In order to determine the dominant reaction mechanism at elevated temperatures, transition path sampling simulations at a realistic reaction temperature (T = 800 K) have been performed. The initial reactive trajectory was obtained by integrating the equations of motion forward and backward, starting from one of the potential-energy saddle points determined previously and using randomly generated Boltzmann-distributed momenta. The type of trial move has been chosen randomly with 80% likelihood of selecting the shooting and 20% of selecting the shifting move. The length of trajectories was fixed to 200 fs, which has been found to be sufficient to capture the whole reaction. The simulation temperature was set to T = 800 K. Reactant and product

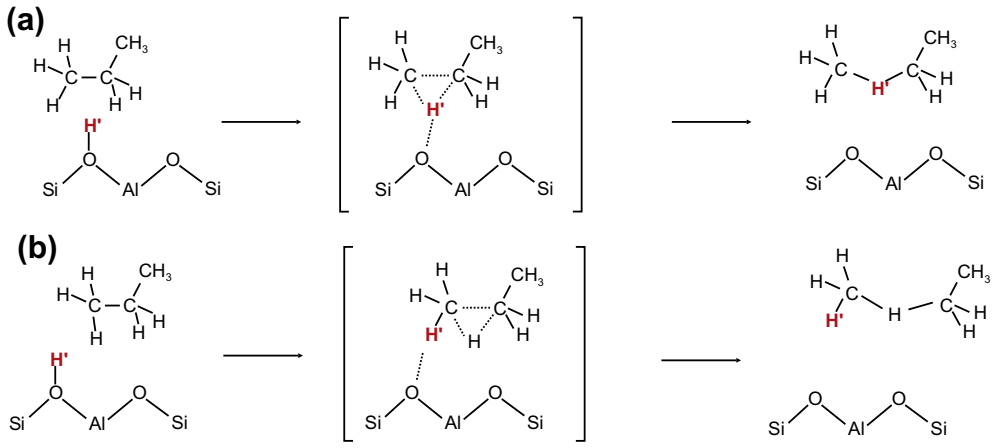

Scheme 2. Two possible realizations of the first reaction step of protolytic cracking of propane. Proton initially sitting at Brønsted acid site is indicated by prime (H′).

states were distinguished using coordinates measuring the O–H′, C–H, and C–C distances. A configuration was identified as a reactant state if the O–H′ distance was shorter than 1.05 Å and the lengths of the two C–C bonds were shorter than 1.7 Å. Similarly, product configurations are defined as structures in which the proton (initially attached to a framework oxygen) was bound to a carbon atom (such that a carbonium cation was created) and one of the C–C bonds was elongated to 1.8 Å or more. Altogether 4000 TPS steps have been performed, producing 1400 different reactive trajectories.

In our TPS simulations, both alternatives for the rate-determining step of protolytic cracking explained in Scheme 2 have been sampled. Note that the mechanism (a) requires that the proton located initially on the framework oxygen (H′) forms bonds with both a methyl group and the methylene group, whereas in mechanism (b), the proton is attached only to the methyl group. The two mechanisms can be therefore distinguished by measuring the difference between two interatomic separations (Δ): the distance between the proton and the carbon in the methylene group and the distance between the proton and the methyl group. The time evolution of the parameter Δ measured for the identified reactive trajectories is shown in Fig. 5. Clearly, two 'stripes' of trajectories can be recognized: those with $\Delta_{t=200} \approx 0$ Å correspond to mechanism (a) and those in which $\Delta_{t=200}$ oscillates around 1.8 Å correspond to mechanism (b). The distribution of the values $\Delta_{t=200}$ is shown in the right panel of Fig. 5. Clearly, mechanism (b) is dominant and we estimate that it determines ~80% of the reactive trajectories.

Fig. 6 shows projections of the configuration space sampled by TPS onto three internal parameters characterizing the cracking reaction: (i) the distance between the framework oxygen at which the proton is located at $t = 0$ and a carbon atom in the methyl group active in the reaction (r_1), (ii) the distance between the proton and the framework oxygen atom (r_2), and (iii) the distance between the two carbon atoms forming the C–C bond that is broken during the reaction (r_3). In all reactant configurations, the parameters r_2 and r_3 correspond to chemical bonds fluctuating around ~0.99 Å and 1.55 Å, respectively. As we have seen in the previous section, the adsorption complexes between propane and the Brønsted acid site are unstable at a reaction temperature of 800 K and r_1 varies between 2.7 and 5 Å. Note that the values of r_1 sampled in TPS are limited by the length of the reactive trajectories restricted to 200 fs in this study. As follows from our analysis of straightforward MD simulations performed at 800 K, the parameter r_1 can even take values larger than 6 Å, see Fig. 4. As the reaction proceeds, the O–H bond and one of the C–C bonds are broken. The reaction

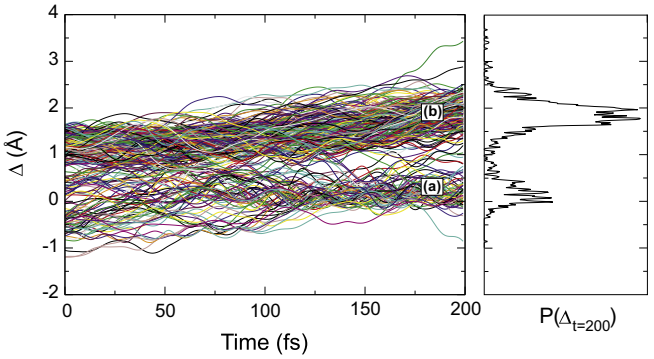

Fig. 5. Time evolution of parameter Δ (distance between proton and carbon in methyl group minus distance between proton and carbon in methylene group) sampled by transition path sampling at $T = 800$ K (left) and the distribution function computed for final points of reactive trajectories $\Delta_{t=200}$ (right). The branches (a) and (b) in left panel correspond to two reaction mechanisms shown in Scheme 1.

intermediate spans a rather broad region of configuration space. The transformation from reactant to reaction intermediate can proceed only through a rather narrow region in configuration space (the space between the two boxes showing the regions characteristic for stable states displayed in Fig. 6). The static transition state configurations (see Section 3) fall into this region (see full red circles in Fig. 6). These results show that the number of possible transition states is smaller than that of reactant and product configurations. In other words, our TPS simulations indicate that the entropy is lower in the transition region than in the reactant state and that the entropy of activation is negative. This effect is quantitatively analyzed using the thermodynamic integration technique in the following section.

6. Calculation of intrinsic reaction parameters

Calculations of the free energy of activation have been made using the thermodynamic integration technique [44–47], described in Appendix A. For the thermodynamic integration, a set of internal coordinates must be chosen such as to form a sufficiently complete basis for the description of the reaction path, i.e., it should contain all essential degrees of freedom which are modified during the reaction. In the present calculations, a set of four coordinates have been used: (i) the distance between the proton and an oxygen atom next to the aluminum framework atom (ξ_1), (ii) the length of the bond between the two carbon atoms C_i

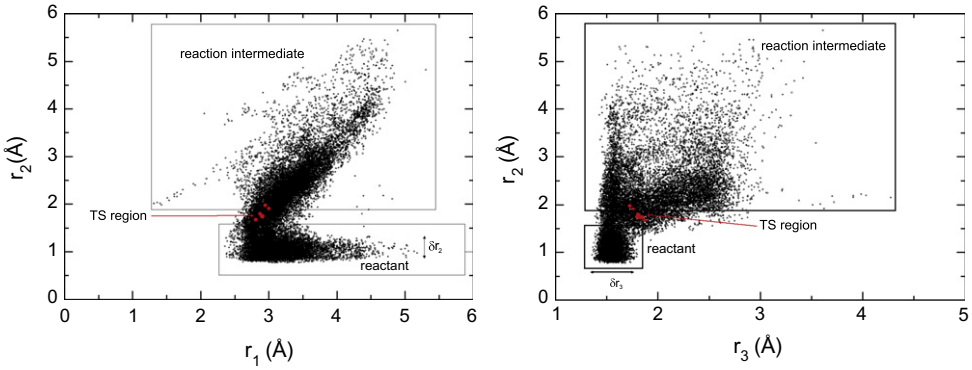

Fig. 6. Configuration space sampled by transition path sampling at T = 800 K projected into set of internal coordinates: distance between framework oxygen atom in Brønsted acid site and carbon in the methyl group that is active in the reaction (r_1), distance between proton and oxygen atom in Brønsted acid site (r_2), and the distance between two carbon atoms forming the C–C bond that is broken during the reaction (r_3). The rectangular boxes indicate typical reactant and intermediate configurations, the area between boxes corresponds to a transition region. Red circles represent static transition states obtained using atomic relaxations. Symbols δr_2 and δr_3 stand for magnitude of thermal vibrations of corresponding internal parameters in the reactant state.

and C_j that is broken during the cracking reaction (ξ_2), and (iii, iv) the coordination numbers for the atoms C_i and C_j by hydrogen atoms (ξ_3 and ξ_4). Following Ref. [54], we characterize the coordination number $cn(C_i)$ for the carbon atom C_i by the continuous function:

$$cn(C_i) = \sum_{l=1}^{N_H} \frac{1 - \left(\frac{r_{C_i-H_l}}{R_0}\right)^9}{1 - \left(\frac{r_{C_i-H_l}}{R_0}\right)^{14}}, \tag{4}$$

where the parameter R_0 is set to 1.5 Å, $r_{C_i-H_l}$ is the distance between atoms C_i and H_l, and the summation is over all hydrogen atoms H_l attached to atoms C_i or C_j (forming the C–C bond to be broken), plus the proton initially located at the Brønsted acid site. Note that altogether six C–H distances contribute to each coordination number.

The free-energy minima in the collective variable space corresponding to the reactant – propane adsorbed in H-chabazite – have been obtained by analyzing the data of the molecular dynamics simulations at T = 800 K. As proposed by Fleurat–Lessard and Ziegler [47], the free-energy transition states have been identified by performing optimizations on the free-energy hypersurface. Free-energy gradients along a path connecting initial and transition state have been determined using constrained ab initio MD simulations, see Eq. (A3) in Appendix A. The simulation time for one free-energy gradient calculation was 50 ps and the simulations have been stopped when each component of the free-energy gradient decreased below a threshold of 0.1 eV/Å (for ξ_1 and ξ_2) or 0.1 eV/(unit coordination number) for ξ_3 and ξ_4. In Table 2, the internal coordinates defining the free-energy minimum and transition state are compared with those for stationary states on the potential energy surface determined by atomic relaxations. The parameters ξ_1–ξ_4 characterizing the free-energy transition state fall into the interval of values found for the static transition states. In the case of the free-energy minimum, the values for parameters ξ_3 and ξ_4 are lower compared to configurations identified in static relaxations. The reason is that the distances between the proton and carbon atoms increase due to thermal effect and the corresponding contribution to the coordination number is smaller (cf. Eq. (4)).

The free-energy profile as a function of the length of the reaction path s is shown in Fig. 7. The computed free-energy barrier is 237 ± 6 kJ/mol. This value is by 26 to 49 kJ/mol higher than the potential energy barriers computed in the static approach. The internal energy of activation has been computed as the difference between the internal energy for the transition state and for the free-energy minimum. Using the constrained molecular dynamics,

Table 2
Internal parameters ξ_1–ξ_4 describing reaction path computed for potential and free-energy stationary states.

	ξ_1	ξ_2	ξ_3	ξ_4
	Relaxations			
Minimum	0.98–0.99	1.53–1.54	3.26–3.31	2.35–2.36
Saddle point	1.68–2.00	1.71–1.87	3.92–4.00	2.90–2.97
	Molecular dynamics, T = 800 K			
Minimum	0.99	1.55	3.12	2.32
Saddle point	1.75	1.76	3.92	2.96

the internal energy of a state with a fixed value of the internal coordinates ξ can be calculated using

$$U(\xi) = \frac{\langle |\mathbf{Z}|^{-1/2} H_{\xi^*} \rangle_{\xi^*}}{\langle |\mathbf{Z}|^{-1/2} \rangle_{\xi^*}}, \tag{5}$$

where H_{ξ^*} is the Hamiltonian of the system and $\mathbf{Z}$ is defined in Eq. (A2).

The calculated value of the internal energy of activation $\Delta U^{\ddagger}$ = 180 kJ/mol is slightly lower than the potential energy barriers computed using the static approach which fall into the interval 188–211 kJ/mol, see Section 3. The entropy of activation can be found using the thermodynamic relation:

$$\Delta A = \Delta U - T\Delta S. \tag{6}$$

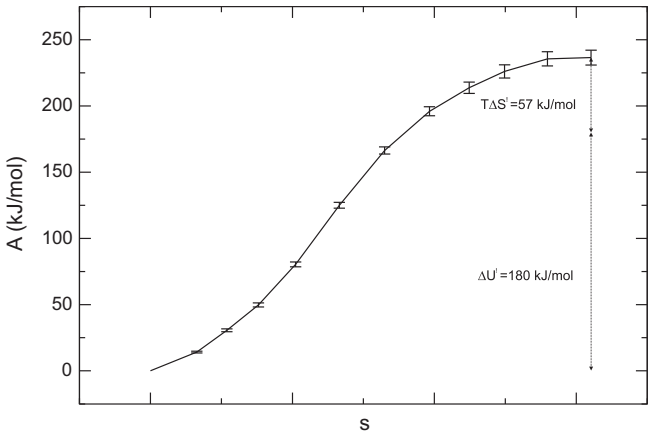

Fig. 7. Free-energy profile for the rate-determining step of monomolecular cracking of propane as a function of path length s. The internal energy ($\Delta U^{\ddagger}$) and entropy ($T\Delta S^{\ddagger}$) contributions are indicated.

The intrinsic entropy of activation has been found to be negative ($\Delta S^{\ddagger}$ = −71 J/mol/K), consistent with our qualitative analysis based on sampling of reactive trajectories discussed in Section 5. A similar result has been reported in the recent theoretical study by Swisher et al. [25] who found that the entropy of activation of the first step of reaction vary between −34 and −71 J/mol/K, depending on chosen structural model and level of theory.

The experimentally measured entropy of activation ranges between −91 to −99 J/K/mol, depending on type of acidic zeolite [14]. It should be noted, however, that this measured value is only an effective parameter which, in addition to entropy of activation, includes also contributions from other physico-chemical processes such as adsorption, diffusion, and desorption of reactant and product molecules. Hence, the relation between the measured and intrinsic entropy of activation is not straightforward. Some authors [13,14] estimated the intrinsic reaction parameters using a Langmuir adsorption model in which the concentration of the reactant state is proportional to the external pressure of reactant (p_B) and the rate of reaction r is defined as

$$r = k_{int} K_B p_B, \tag{7}$$

where k_{int} and K_B are the intrinsic rate of reaction and adsorption constant, respectively. In this model, it is implicitly assumed that once an alkane is adsorbed, it is immediately in a 'reactant' state, i.e., it forms an adsorption complex with the Brønsted site. This model yields simple relations between measured, intrinsic, and adsorption parameters:

$$E^{\ddagger}_{meas} = E^{\ddagger}_{int} + \Delta H_{ads}, \tag{8}$$

$$\Delta S^{\ddagger}_{meas} = \Delta S^{\ddagger}_{int} + \Delta S_{ads}. \tag{9}$$

The intrinsic entropy of activation for propane predicted using this model has small negative value (−9 J/mol/K). For longer linear alkanes, predicted $\Delta S^{\ddagger}_{int}$ is even positive. Clearly, this simple model assumes that reactant looses most of entropy when shifting from gas phase to adsorbed state, which is implicitly identified with adsorption complex, i.e., reactant bound to the active site. The picture arising from our simulations and also from the recent theoretical work of Swisher et al. [25] is distinctly different: the propane molecule is not strongly bound to the active site in the adsorbed state at T = 800 K; instead, it can almost freely move and rotate in the zeolite cavity. In other words, a reactant bound to the BA site cannot be considered to be a typical adsorption state configuration. Consequently, the entropy loss due to adsorption predicted by the simulations [25] (−20 to −40 J/mol/K) is significantly lower than assumed in Refs. [13,14] (−102 J/mol/K). Our simulations show that the formation of an adsorption complex in which propane gets close enough to active site to be activated is an integral part of the cracking process.

7. Conclusions

Propane cracking has been studied using periodic density functional calculations and ab initio molecular dynamics simulations. To account for van der Waals interactions between propane and the zeolite, the semiempirical dispersion corrections proposed by Grimme [37] have been used. The internal energy of adsorption of −44 kJ/mol computed using molecular dynamics at T = 300 K is comparable with the experimental heat of adsorption measured for a zeolite with similar framework density as in chabazite (−47 kJ/mol). Our ab initio molecular dynamics simulations show that propane forms stable reactant complexes with a Brønsted acid site only at low temperatures. The probability to form a reactant complex decreases with temperature: at T = 800 K, the typical reaction temperature for protolytic cracking, thermal disorder dominates over the weak specific interaction between propane and the Brønsted acid site. A very similar behavior – a decreased probability to form a reactant complex at higher temperature – has been reported by Swisher et al. [25] who studied the adsorption thermodynamics of alkanes in zeolites using Monte Carlo simulation techniques combined with empirical force fields.

Transition path sampling has been used to determine the reaction mechanism for the rate-determining step of propane cracking. It has been shown that both possible reaction mechanisms (Scheme 2) contribute to cracking with significant, but distinctly different probability. The dominant mechanism is the one shown in Scheme 2b (∼80% of reactive trajectories) in which the proton is attached to a methyl group and another hydrogen atom is shifted toward the carbon in the CH_2 group to form a C–H bond and at the same time the bond between the methyl and methylene groups is broken. The lower probability of mechanism (a) – direct proton attack on a C–C bond – arises from the fact that this mechanism requires a specific orientation of the propane molecule with respect to the Brønsted acid site in which both the methyl and methylene groups are close to the proton. In mechanism (b), on the other hand, only one methyl group interacts with Brønsted site, leading to an enhanced flexibility of the reactant configuration. Mechanism (a) is therefore disfavored by entropy effects.

The intrinsic reaction parameters such as free energy, entropy, and internal energy of activation have been determined using the thermodynamic integration technique. The computed free and internal energies of activation are 237 kJ/mol and 180 kJ/mol, respectively, the latter value being comparable with potential energy barriers computed using the static approach. The computed entropy of activation of −71 J/mol/K is close to result of Swisher et al. [25] who reported the value of −68 J/mol/K computed using a plane-wave DFT method similar to the present calculations. The experimental value of $\Delta S^{\ddagger}$ ranges between −91 and −99 J/K/mol, depending on type of acidic zeolite [14].

In this work, we provided evidence that finite temperature effects are important at various stages of the cracking process. Ab initio molecular dynamics simulations have demonstrated that at elevated temperatures the adsorption energy is substantially lower than the value determined from the energy minimum on the static potential energy surface. In addition, these simulations demonstrate that at typical reaction temperatures only a small fraction of the molecules adsorbed in the zeolite form a reactant complex for protonation. Transition path sampling has been used to determine the dominant reaction mechanism, demonstrating that reactions via protonation of a terminal methyl group are far more frequent than the direct attack of the acidic proton on a C–C bond (which has been assumed in most previous DFT studies). Thermodynamic integration shows that the free energy of activation is higher than the static potential energy barrier, caused by the loss of entropy in the transition state configurations.

Finally, it should be mentioned that alkanes undergo also other kinds of chemical transformations, in particular dehydrogenation, at reaction conditions typical for protolytic cracking [8,12,14]. In our previous study [50], we have estimated potential energy barriers of 256 and 206 kJ/mol for the propane dehydrogenation involving methyl and methylene groups, respectively. Evidently, the barrier for the reaction involving methylene group is comparable with the values identified for the propane cracking, see Table 1. This result is consistent with the experimentally observed fact that the rate of dehydrogenation is typically lower but comparable to that for cracking. Combined with the striking similarity in the mechanism of the first reaction step (proton transfer), this result suggests that both competing reactions could be studied in a single TPS simulation. Note, however, that the cracking reaction requires proton transfer to the methyl group, whereas the energetically favorable route for dehydrogenation involves H transfer to the methylene group of propane [50]. Obviously, an efficient sampling

of both competing reactions would require many changes of proton acceptor sites in propane during the TPS run. In our TPS study of propane dehydrogenation [50], ~1200 TPS steps were needed to switch the reaction mode from the methyl dehydrogenation to the methylene dehydrogenation. It can be therefore expected that sampling over very large number of reactive trajectories would be needed to study both cracking and dehydrogenation in a single TPS simulation. We plan to address this very interesting topic in our future work.

Acknowledgments

This work has been supported by the VASP project. The use of facilities at Computing Center of Vienna University is kindly acknowledged.

Appendix A. Thermodynamic integration

In general, if molecular dynamics with constrained vector of geometric parameters $\xi = \{\xi_k;\ k = 1,\ldots,r\}$ is performed, correct statistical average for a quantity $a(\xi)$ can be obtained using the formula:

$$a(\xi) = \frac{\langle |\mathbf{Z}|^{-1/2} a(\xi^*)\rangle_{\xi^*}}{\langle |\mathbf{Z}|^{-1/2}\rangle_{\xi^*}}, \tag{A1}$$

where $\langle \ldots \rangle_{\xi^*}$ stands for statistical average of a quantity enclosed in angular parentheses computed for a constrained ensemble and $\mathbf{Z}$ is a mass metric tensor defined as:

$$Z_{\alpha,\beta} = \sum\nolimits_{i=1}^{i=M} \frac{1}{m_i} \frac{\partial \xi_\alpha}{\partial x_i} \frac{\partial \xi_\beta}{\partial x_i}, \alpha = 1,\ldots,r, \beta = 1,\ldots,r, \tag{A2}$$

It can be shown [44–47] that the free-energy gradient can be computed using equation:

$$\left(\frac{\partial A}{\partial \xi_k}\right)_{\xi^*} = \frac{1}{\langle |\mathbf{Z}|^{-1/2}\rangle_{\xi^*}} \langle |\mathbf{Z}|^{-1/2} [-\lambda_{\xi_k} + \frac{k_B T}{2|\mathbf{Z}|} \sum_{j=1}^{j=r} (\mathbf{Z}^{-1})_{kj} \sum_{i=1}^{i=M} \frac{1}{m_i} \frac{\partial \xi_j}{\partial x_i} \frac{\partial |\mathbf{Z}|}{\partial x_i}] \rangle_{\xi^*}, \tag{A3}$$

where λ_{ξ_k} is Lagrange multiplier associated with the parameter ξ_k used in the SHAKE algorithm [55].

The free-energy difference between states (1) and (2) can be computed by integrating free-energy gradients over a connecting path:

$$\Delta A_{1\to 2} = \int_{\xi(1)}^{\xi(2)} \left(\frac{\partial A}{\partial \xi}\right)_{\xi^*} \cdot d\xi. \tag{A4}$$

Note that as free energy is a state quantity, the choice of path connecting (1) with (2) is irrelevant. If the initial and final states are chosen to be free-energy minimum and saddle point, respectively, free-energy barrier can be computed using Eq. (A4).

Appendix B. Transition path sampling

In transition path sampling (TPS) [49], random walk in the space of reactive trajectories is performed. In this context, a reactive trajectory is a sequence of states, i.e., reaction coordinates and the conjugate momenta, that connects configuration space regions typical for reactants (A) and products (B) which can be distinguished using a suitably chosen geometric parameter such as bond length, coordination number. A sampling in reactive trajectory space is realized via trial moves, called "shooting" and "shifting". If a new trajectory generated by a trial move still connects A with B, it is accepted and it is used for the next iteration. In the opposite case, the trajectory is rejected and simulation continues using the previous reactive trajectory. In a "shooting" trial move, a state *i* on the current trajectory is selected randomly and the corresponding momenta are modified by adding a small Boltzmann-distributed noise. A new trajectory is generated by integrating equations of motion forward and backward in time. In a "shifting" move, a state *i* from a region typical for A (or B) is chosen, all states before (after) *i* on the trajectory are discarded and the same number of states is added at the other end of trajectory by continued integration of the equations of motion. Note that the length of trajectories is fixed in a typical TPS simulation. For in-depth description of TPS technique, see Ref. [49].

References

[1] H. Maxwell, W. Stork, Introduction to Zeolite Science and Practice, Elsevier, Amsterdam, 1991.
[2] B. Greensfelder, H. Voge, G. Good, Ind. Eng. Chem. 41 (1949) 2573.
[3] C. Thomas, Ind. Eng. Chem. 41 (1949) 2564.
[4] W.O. Haag, R.M. Dessau, in: Proceedings of the 8th International Congress of Catalysis, Berlin, 2–6 July 1984, vol. 2, Verlag Chemie, Weinheim, 1984.
[5] S. Altwasser, C. Welker, Y. Traa, J. Weitkamp, Micropor. Mesopor.Mater. 83 (2005) 345–356.
[6] H. Krannila, W. Haag, B. Gates, J. Catal. 135 (1992) 115–124.
[7] T. Narbeshuber, H. Vinek, J. Lercher, J. Catal. 157 (1995) 388–395.
[8] T. Narbeshuber, A. Brait, K. Seshan, J. Lercher, J. Catal. 172 (1997) 127.
[9] F. Jentoft, B. Gates, Top. Catal. 4 (1997) 1–13.
[10] J. van Bokhoven, B. Williams, W. Ji, D. Koningsberger, H. Kung, J. Miller, J. Catal. 224 (2004) 50–59.
[11] C. Ramachadran, B.A. Williams, J.A. Van Bokhoven, J.T. Miller, J. Catal. 233 (2005) 100–108.
[12] B. Xu, C. Sievers, S.B. Hong, R. Prins, J.A. van Bokhoven, J. Catal. 244 (2006) 163.
[13] A. Bhan, R. Gounder, J. Macht, E. Iglesia, J. Catal. 253 (2008) 221–224.
[14] R. Gounder, E. Iglesia, J. Am. Chem. Soc. 131 (2009) 1958–1971.
[15] S. Collins, P. O'Malley, J. Catal. 153 (1995) 94–99.
[16] S. Collins, P. O'Malley, Chem. Phys. Lett. 246 (1995) 555–561.
[17] S. Blaszkowski, M. Nascimento, R. vanSanten, J. Phys. Chem. 100 (1996) 3463.
[18] S. Blaszkowski, R. vanSanten, Top. Catal. 4 (1997) 145.
[19] A. Rigby, G. Kramer, R. van Santen, J. Catal. 170 (1997) 1–10.
[20] M. Boronat, P. Viruela, A. Corma, Phys. Chem. Chem. Phys. 2 (2000) 3327.
[21] S. Zygmunt, L. Curtiss, P. Zapol, L. Iton, J. Phys. Chem. B 104 (2000) 1944.
[22] X. Zheng, P. Blowers, J. Mol. Catal. A 229 (2005) 77–85.
[23] X. Zheng, P. Blowers, J. Phys. Chem. A 109 (2005) 10734.
[24] X. Zheng, P. Blowers, J. Phys. Chem. A 110 (2006) 2455.
[25] J.A. Swisher, N. Hansen, T. Maesen, F.J. Keil, B. Smit, A.T. Bell, J. Phys. Chem. C 114 (2010) 10229–10239.
[26] L. Benco, T. Demuth, J. Hafner, F. Hutschka, H. Toulhoat, J. Chem. Phys. 114 (2001) 6327.
[27] Y. Jeanvoine, J. Ángyán, G. Kresse, J. Hafner, J. Phys. Chem. B 102 (1998) 5573.
[28] S. Zones, R. Van Nostrand, Zeolites 8 (1988) 166.
[29] G. Kresse, J. Hafner, Phys. Rev. B 48 (1993) 13115.
[30] G. Kresse, J. Hafner, Phys. Rev. B 49 (1994) 14251.
[31] G. Kresse, J. Furthmüller, Comput. Mater. Sci. 6 (1996) 15.
[32] G. Kresse, J. Furthmüller, Phys. Rev. B 54 (1996) 11169.
[33] P. Blöchl, Phys. Rev. B 50 (1994) 17953.
[34] G. Kresse, D. Joubert, Phys. Rev. B 59 (1999) 1758.
[35] J.P. Perdew, K. Burke, M. Ernzerhof, Phys. Rev. Lett. 77 (1996) 3865–3868.
[36] F. Eder, J. Lercher, Zeolites 18 (1997) 75.
[37] S. Grimme, J. Comput. Chem. 27 (2006) 1787.
[38] T. Bucko, J. Hafner, S. Lebegue, J.G. Angyan, J. Phys. Chem. A 114 (2010) 11814–11824.
[39] G. Henkelman, H. Jónsson, J. Chem. Phys. 111 (1999) 7010.
[40] A. Heyden, A. Bell, F. Keil, J. Chem. Phys. 123 (2005) 224101.
[41] W.H. Press, B.P. Flannery, S.A. Teukolsky, W.T. Vetterling, Numerical Recipes in FORTRAN 77: The Art of Scientific Computing, second ed., vol. 1, Cambridge University Press, 1992.
[42] S. Nosé, J. Chem. Phys. 81 (1984) 511.
[43] W. Hoover, Phys. Rev. A 31 (1985) 1695.
[44] E. Carter, G. Ciccotti, J. Hynes, R. Kapral, Chem. Phys. Lett. 156 (1989) 472.
[45] W. Den Otter, W. Briels, Mol. Phys. 98 (2000) 773–781.
[46] E. Darve, M. Wilson, A. Pohorille, Mol. Simul. 28 (2002) 113.
[47] P. Fleurat-Lessard, T. Ziegler, J. Chem. Phys. 123 (2005).
[48] T. Bucko, L. Benco, J. Hafner, J.G. Ángyán, J. Catal. 250 (2007) 171.
[49] C. Dellago, P. Bolhuis, P. Geissler, Adv. Chem. Phys. 123 (2002) 1.
[50] T. Bucko, L. Benco, O. Dubay, C. Dellago, J. Hafner, J. Chem. Phys. 131 (2009).
[51] V. Kazansky, M. Frash, R. van Santen, Catal. Lett. 28 (1994) 211.
[52] F. Eder, J. Lercher, J. Phys. Chem. B 101 (1997) 1273.
[53] F. Eder, M. Stockenhuber, J. Lercher, J. Phys. Chem. B 101 (1997) 5414.
[54] M. Iannuzzi, A. Laio, M. Parrinello, Phys. Rev. Lett. 90 (2003) 238302.
[55] J. Ryckaert, G. Ciccotti, H. Berendsen, J. Comput. Phys. 23 (1977) 327.